Journal of Molecular Structure 1098 (2015) 365–376

Contents lists available at ScienceDirect

Journal of Molecular Structure

journal homepage: http://www.elsevier.com/locate/molstruc

Synthesis and structure investigation of novel pyrimidine-2,4,6-trione derivatives of highly potential biological activity as anti-diabetic agent

Assem Barakat [a, b, *], Saied M. Soliman [b], Abdullah Mohammed Al-Majid [a], Gehad Lotfy [c], Hazem A. Ghabbour [d], Hoong-Kun Fun [d, e], Sammer Yousuf [f], M. Iqbal Choudhary [a, f], Abdul Wadood [g]

[a] Department of Chemistry, College of Science, King Saud University, P.O. Box 2455, Riyadh 11451, Saudi Arabia
[b] Department of Chemistry, Faculty of Science, Alexandria University, P.O. Box 426, Ibrahimia, Alexandria 21321, Egypt
[c] Organic Chemistry Department, Faculty of Pharmacy, Suez Canal University, Ismailia, Egypt
[d] Department of Pharmaceutical Chemistry, College of Pharmacy, King Saud University, P.O. Box 2457, Riyadh 11451, Saudi Arabia
[e] X-Ray Crystallography Unit, School of Physics, Universiti Sains Malaysia, Penang 11800, Malaysia
[f] H.E.J. Research Institute of Chemistry, International Center for Chemical Sciences, University of Karachi, Karachi 75270, Pakistan
[g] Department of Biochemistry, Abdul Wali Khan University Mardan, Mardan 23200, Pakistan

ARTICLE INFO

Article history:
Received 3 May 2015
Received in revised form
9 June 2015
Accepted 11 June 2015
Available online 15 June 2015

Keywords:
Pyrimidine-2,4,6(1*H*,3*H*,5*H*)-trione
Barbituric acid
DFT computations
α-Glucosidase inhibition
Post-prandial hyperglycemia
Molecular docking

ABSTRACT

Synthesis of (±)-1,3-dimethyl-5-(1-(3-nitrophenyl)-3-oxo-3-phenylpropyl)pyrimidine-2,4,6(1*H*,3*H*,5*H*)-trione (**3**) is reported. The structure of compound **3** was deduced by using spectroscopic methods, X-ray crystallography, and DFT calculations. The calculated geometric parameters were found to be in good agreement with the experimental data obtained from the X-ray structure. The NBO calculations were performed to predict the natural atomic charges at the different atomic sites and to study the different intramolecular charge transfer (ICT) interactions. The high LP(3)O6 →z BD*(2)O5–N3 ICT interaction energy (165.36 kcal/mol) indicated very strong n → π* electron delocalization while the small LP(2) O → BD*(1)C–H ICT interaction energies indicated that the C–H … O intramolecular interactions are weak. The ^{1}H and ^{13}C NMR chemical shifts calculated using GIAO method showed good agreement with the experimental data. The calculated electronic spectra of the studied compound using TD-DFT method showed intense electronic transition band at 243.9 nm (f = 0.2319) and a shoulder at 260.2 nm (f = 0.1483) which were due to H-4/H-2/H-1/H → L+2 and H-5 → L electronic excitations, respectively. Compound **3** (IC_{50} = 305 ± 3.8 μM) was identified as a potent inhibitor of α-glucosidase *in vitro* and showed several fold more inhibition than the standard drug acarbose (IC_{50} = 841 ± 1.73 μM). Molecular docking of the synthesized compound was discussed.

1. Introduction

Nitrogen-containing compounds are privileged heterocyclic scaffold due to their biological and pharmaceutical activities [1]. For example, pyrimidine-2,4,6-trione derivatives are known to have as anti-hypertensive [2], anti-cancer [3], anti-convulsant [4] anti-inflammatory [5], and anti-psychotic properties [6]. Because of the biological activities of these compounds, pyrimidine-2,4,6-triones (PYT) are widely used as a synthons in the design of antitumor agents. They have high efficacy to form hydrogen-bonding with drug targets (1–4, Fig. 1) [7–10]. Singh et al. have evaluated a series of new *N*-benzyl indole-pyrimidine-2,4,6-trione hybrid molecules against a panel of 60 human tumor cell lines. Several of these analogs are also inhibitors of DNA repair and replication stress response polymerases [11]. Recently, Barakat et al. [12], synthesized and evaluated some novel zwitterionic adduct derived from pyrimidine-2,4,6-trione (*e.g.*, compound **5**, Fig. 1) possess anti-oxidant properties.

Named after Arthur Michael, the conjugate addition of nucleophiles to acceptor activated alkene and alkyne substrates is a recognized strategy for an efficient and versatile construction of C–C bonds. The reaction produces a large variety of the conjugate addition products based on a broad range of the Michael donors

* Corresponding author. Department of Chemistry, College of Science, King Saud University, P. O. Box 2455, Riyadh 11451, Saudi Arabia.
E-mail address: ambarakat@ksu.edu.sa (A. Barakat).

http://dx.doi.org/10.1016/j.molstruc.2015.06.037
0022-2860/

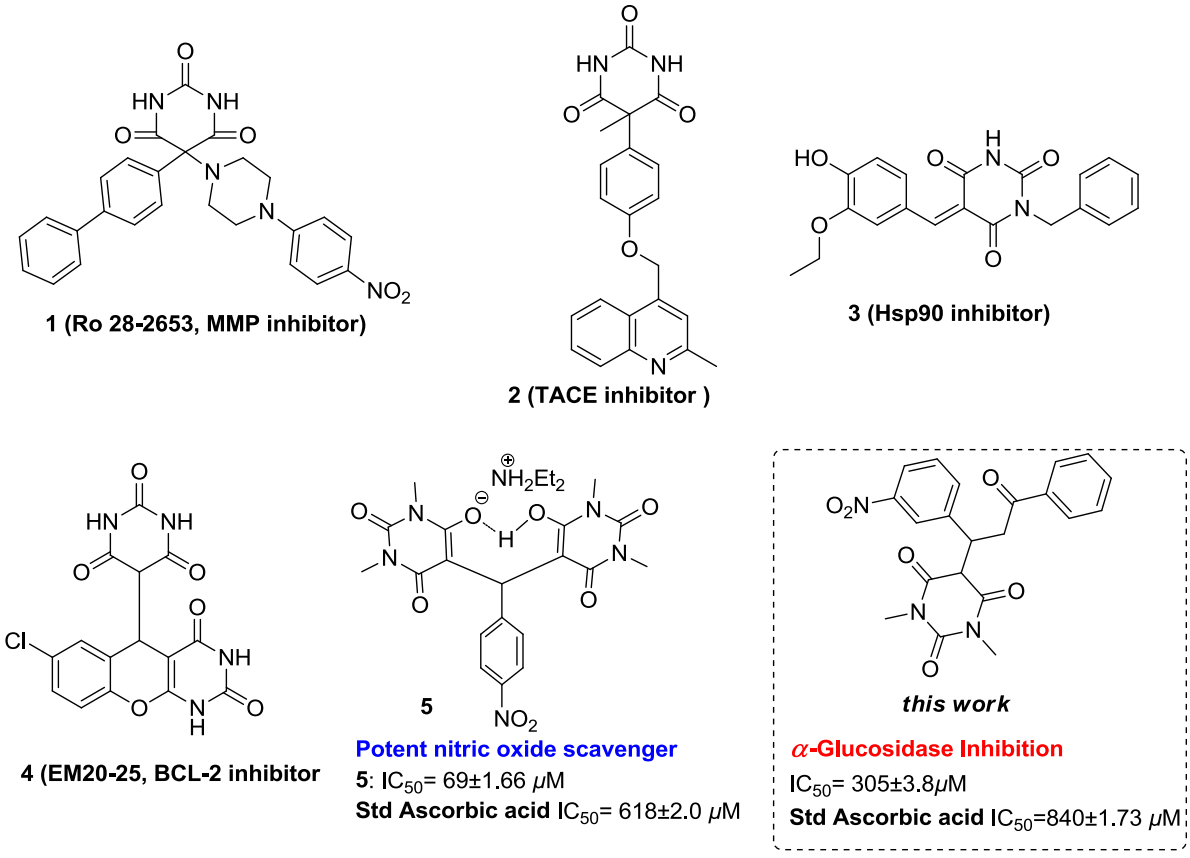

Fig. 1. Anticancer agents and anti-oxidant bearing pyrimidine-2,4,6-trione moiety.

and acceptor. Depending upon the nature of the nucleophile, many of its variants, in the form of hetero-Michael reactions, whose recent examples include, the sulpha-Michael, aza-Michael, oxo-Michael and phospha-Michael have been developed. The classical Michael additions are typically base catalyzed that also promotes Michael adducts efficiently [13–26].

In view of these reports and our interest in the synthesis of bioactive heterocyclic compounds [27–32], we report here an efficient synthesis of 1,3-dimethyl-5-(1-(3-nitrophenyl)-3-oxo-3-phenylpropyl)pyrimidine 2,4,6(1*H*,3*H*,5*H*)–trione. DFT/B3LYP calculations have also been performed to study the molecular structure characteristics of the studied compound. The electronic and spectroscopic properties of the compound have been predicted using the same level of theory. The TD-DFT calculations were used to predict and assign the electronic spectra of the studied compound. NBO calculations were performed to predict the natural atomic charges, and to study the different intramolecular charge transfer (ICT) interactions occurring in the studied system. The NMR chemical shifts were calculated using the gauge including atomic orbital (GIAO) method and used to assign the experimental results.

2. Experimental

2.1. General remarks

All the glassware was oven–dried before use, and the reactions were conducted under inert atmosphere. The progress of the reaction was monitored by TLC (Merck Silica Gel 60 F–254 thin layer plates). The chemicals were purchased from Aldrich, and Fluka etc, and were used without further purification, unless otherwise stated. Petroleum ether (PE), hexane, and ethyl acetate were distilled prior to use, especially for column chromatography. All the major solvents were dried by using slandered drying techniques mentioned in the literature. Melting points were measured on a Gallen-kamp melting point apparatus in open glass capillaries and are uncorrected. IR Spectra were measured as KBr pellets on a Nicolet 6700 FT-IR spectrophotometer. The NMR spectra were recorded on a Jeol-400 NMR spectrometer. ^{1}H NMR (400 MHz), and ^{13}C NMR (100 MHz) were run in deuterated chloroform ($CDCl_3$). Chemical shifts (δ) are referred in terms of *ppm* and *J* -coupling constants are given in *Hz*. Mass spectrometric analysis was conducted by using ESI mode on AGILENT Technologies 6410–triple quad LC/MS instrument. Elemental analysis was carried out on Elmer 2400 Elemental Analyzer, CHN mode. The X-ray diffraction measurement of compound **3** was collected by using Bruker SMART APEXII D8 Venture diffractometer. The thermal analysis of the studied compound has been carried out using TGA Q500 V20.10. The wt% loss has been measured from the ambient temperature up to 800 °C.The electronic spectrum of the studied compound is measured using Perkin Elmer, Lambda 35, UV/Vis spectrophotometer.

3 (Ethanol): 205 nm, 243 nm and 266 nm (sh).

2.2. 1,3-Dimethyl-5-(1-(3-nitrophenyl)-3-oxo-3-phenylpropyl) pyrimidine-2,4,6- (1H,3H,5H)-trione (**3**)

A solution of *N*,*N*-dimethyl barbituric acid **1** (1.5 mmol) and enone derivatives **2** (1.5 mmol) in 2 mL of dry CH_2Cl_2 were charged into a 50 mL round bottom flask under inert atmosphere. The Et_2NH (1.5 mmol) was then added to the reaction mixture and stirred at room temperature for up to 1.5–2 h, until TLC showed complete consumption of both the reactants. After the completion of

reaction, the crud product directly subjected to column chromatography using 100–200 mesh silica gel and ethyl acetate/*n*-hexane (2:8, v/v) as an eluent to afford the racemic mixture of products **3**.

^{1}H NMR (400 MHz, $CDCl_3$) δ: 3.07 (s, 3H, $-NCH_3$), 3.16 (s, 3H, $-NCH_3$), 3.59 & 3.63 (dd, 1H, J = 18.32 Hz, 5.84 Hz, $CH_{2(a)}$), 3.98 (d, 1H, J = 3.68 Hz, CH), 4.05 & 4.10 (dd, 1H, J = 18.32 Hz, 8.08 Hz, $CH_{2(e)}$), 4.45–4.55 (m, 1H, CH), 7.39–7.49 (m, 3H, Ar–H), 7.56 (d, 2H, J = 8.80 Hz, Ar–H), 7.97 (d, 2H, J = 7.36 Hz, Ar–H), 8.06–8.12 (m, 2H, Ar–H); ^{13}C NMR (100 MHz, $CDCl_3$) δ: 28.3, 28.3, 40.5, 42.7, 52.6, 122.3, 123.1, 128.0, 128.7, 129.7, 133.6, 134.3, 136.3, 141.4, 148.3, 150.7, 167.3, 167.4, 197.3; IR (KBr, cm^{-1}) ν_{max} = 3420, 3083, 2953, 1689, 1526, 1449, 1346, 1298, 1270; [Anal. Calcd. for $C_{21}H_{19}N_3O_6$: C, 61.61; H, 4.68; N, 10.26; Found: C, 61.49; H, 4.52; N, 10.11]; LC/MS (ESI, m/z): [M^+], found 409.10, $C_{21}H_{19}N_3O_6$ requires 409.13.

2.3. Single-crystal X-ray diffraction studies

Compound **3** was obtained as crystals by slow diffusion of diethyl ether solution of compounds **3** in dichloromethane at room temperature for 24 h. Diffraction data was collected on a Bruker APEX-II D8 Venture area diffractometer, equipped with graphite monochromatic Cu Kα radiations at 293 (2) °K. Cell refinement and data reduction were carried out by Bruker SAINT. SHELXS-97 [33,34] was used to solve structure. The final refinement was carried out by full-matrix least-squares techniques with anisotropic thermal data for nonhydrogen atoms on 3. All the hydrogen atoms were placed at calculated positions.

The structure of **3** was determined by X-ray crystal structure analysis (Bruker AXS GmbH). CCDC- 1024287; contains the supplementary crystallographic data for this compound. These data can be obtained free of charge from the Cambridge Crystallographic Data Centre via www.ccdc.cam.ac.uk/data_request/cif.

2.4. α-Glucosidase inhibition assay

Glucosidase inhibition assay was performed spectrophotometrically. α-Glucosidase from *Saccharomyces cerevisiae* (G0660-750UN, Sigma Aldrich) was dissolved in phosphate buffer (pH 6.8., 50 mM). Compound **3** was dissolved in 70% DMSO. In 96-well plates, 20 μL of test compound, 20 μL of enzyme and 135 μL of buffer were added, and incubated for 15 min at 37 °C. After incubation, 25 μL of *p*-nitrophenyl-α-D-glucopyranoside (0.7 mM, Sigma Aldrich) was added and change in absorbance was monitored for 30 min at 400 nm. Test compound was replaced with DMSO (7.5% final) as a control. Acarbose (Sigma Aldrich) was used as a standard inhibitor.

2.5. Computational study

All the quantum chemical calculations of the studied compound were performed by applying DFT method with the B3LYP functional and 6–311G (d,p) basis set using Gaussian 03 software [35]. The input file was taken from the CIF obtained from the X–ray single crystal measurement. The geometry was optimized by minimizing the energies with respect to all the geometrical parameters without imposing any molecular symmetry constraints. GaussView4.1 [36] and Chemcraft [37] programs were used to draw the structure of the optimized geometry. Frequency calculations at the optimized geometry were aimed out to confirm the optimized structure to be an energy minimum. The true energy minimum at the optimized geometry of the studied compound was confirmed by absence of any imaginary frequency modes. The electronic spectra of the studied compound were calculated by the TD–DFT method. The gauge including atomic orbital (GIAO) method was used for the NMR calculations. The ^{1}H and the ^{13}C isotropic shielding tensors referenced to the TMS calculations were carried out at the same level of theory. The natural bond orbital analyses were performed using the NBO calculations as implemented in the Gaussian 03 package [38] at the DFT/B3LYP level.

2.6. Homology modeling and molecular docking study of compound 3

The study was designed to dock compound **3** against α-glucosidase enzyme with the following communications; Intel$^{(R)}$ xenon$^{(R)}$ CPU E5620@2.40GHz system having 3.8 GB RAM with the open 11.4 (X 86_64) operating platform. Protein-Ligand docking was carried out using the Molecular Operating Environment (MOE 2010.11) software package. The three dimensional structure for α-glucosidase of *S. cerevisiae* has not been solved up-to yet, although only few homology models has been reported [39–42]. In the current study we predict 3D structure for α-glucosidase of *S. cerevisiae* by using same protocol as described by (Burke et al.) of homology modeling [42]. The primary sequence of α-glucosidase for *S. cerevisiae* was retrieved from UniProt (Access code P53341). Template search was performed using MOE-Search tools against the PDB implemented in MOE v2010.11. The crystallographic structure of *S. cerevisiae* isomaltase (PDB code 3AJ7; Resolution 1.30 Å) with 72.4% of sequence identity with the target was selected as a template [43]. The 3D structure of α-glucosidase for *S. cerevisiae* was predicted using MOE homology modeling tools. The developed model was then subjected to energy minimization up to 0.05 gradients.

Before docking, ligands and protein were prepared using MOE v2010.11. 3D structure of compound **3** was built by using Molecular Builder Module program implemented in MOE and save as a (.mdb) file for molecular docking. Subsequently, the energy of compound **3** was minimized up to 0.05 Gradient using MMFF 94x force field. *Energy minimization* of the compound **3** was followed by the preparation of protein for docking purposes. Most macromolecular crystal structures contain little or no hydrogen coordinate data due to limited resolution and thus protonation was done prior to docking using Protonate 3D tools. *Protonation* was followed by energy minimization up to 0.05 Gradient using Amber 99 force field. The compound **3** was docked into the active site of protein using the Triangular Matching docking method and 30 conformations of compound **3** and protein complex were generated with docking score (S). The complex was analyzed for interactions and their 3D images were taken by using visualizing tool PyMol.

3. Results and discussion

3.1. Synthesis

The synthetic pathway to the title compound is summarized in Scheme 1. The starting compounds, *N*,*N*-dimethyl barbituric acid (**1**) is commercially available, (*E*)-3-(3-nitrophenyl)-1-phenylprop-2-en-1-one (**2**) was obtained by the condensation of *m*-nitrobenzaldehyde with acetophenone [25,26]. The reaction of (**1**) with equimolar amount of enone **2** in DCM using $NHEt_2$ as a base afforded the target compound **3** in 93% yield. The desired compound (±) 3 was obtained as a racemic mixture. The compound was characterized by a combined application of ^{1}H, and ^{13}C and GC–MS spectroscopy.

3.2. Single − crystal X-ray diffraction study

A specimen of $C_{21}H_{19}N_3O_6$, approximate dimensions 0.367 mm × 0.451 mm × 0.841 mm was used for the X-ray

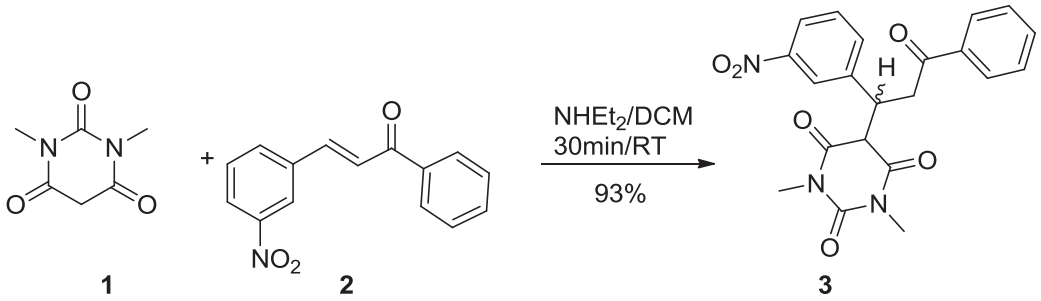

Scheme 1. Michael addition reaction of *N*,*N*-dimethyl barbituric acid **1** into enone derivative **2**.

crystallographic analysis. The integration of the data using a monoclinic unit cell yielded a total of 28249 reflections to a maximum θ angle of 70.13° (0.82 Å resolution), of which 3668 were independent (average redundancy 7.701, completeness = 99.8%, R_{int} = 4.12%, R_{sig} = 2.19%) and 3296 (89.86%) were greater than $2\sigma(F^2)$. The final cell constants of a = 9.5053(2) Å, b = 12.1670(2) Å, c = 17.5962(3) Å, β = 108.3640(10)°, volume = 1931.38(6) Å^3, are based upon the refinement of the XYZ-centroids of reflections above 20 σ(I). The calculated minimum and maximum transmission coefficients (based on crystal size) are 0.5250 and 0.7390 (Table 1.).

The asymmetric unit of compound **3** contains one molecule which composed of three rings; two phenyl rings (C8–C13) and (C14–C19) in addition to pyrimidine ring (C1/N2/C2/N1/C3/C4) as shown in Fig. 2. These three rings form three different planes, the angles between the two phenyl rings is 30.82 (4)°, and the angles between pyridine ring and the(C8–C13) and (C14–C19) phenyl rings are 6.70 (2)°and 37.56 (3)°, respectively. In the crystal; molecules are linked *via* C–H ··· ·O interactions to form parallel chains along the *a*-axis (Fig. 3, Table 3). Only one form "*R*" of resulting racemic product was studied by the single-crystal X-ray diffraction analysis, but the "*S*" form exist in equal amount.

Table 1
Experimental details.

Crystal data	
Chemical formula	$C_{21}H_{19}N_3O_6$
M_r	409.39
Crystal system, space group	Monoclinic, $P_{21/c}$
Temperature (K)	293
a, b, c (Å)	9.5053 (2), 12.1670 (2), 17.5962 (3)
β (°)	108.364 (1)
V (Å^3)	1931.38 (6)
Z	4
Radiation type	Cu Kα
μ (mm−1)	0.88
Crystal size (mm)	0.84 × 0.45 × 0.37
Data collection	
Diffractometer	Bruker APEX-II D8 Venture diffractometer
Absorption correction	Multi-scan SADABS V2012/1 (Bruker AXS Inc.)
T_{min}, T_{max}	0.61, 0.74
No. of measured, independent and observed [I > 2σ(I)] reflections	28249, 3668, 3296
R_{int}	0.041
Refinement	
R[F^2 > 2σ(F^2)], wR(F^2), S	0.050, 0.133, 1.03
No. of reflections	3668
No. of parameters	273
No. of restraints	0
H-atom treatment	H-atom parameters constrained
$\Delta\rho_{max}$, $\Delta\rho_{min}$ (e Å^{-3})	0.32, −0.28

3.3. Biological activity evaluation

Compounds **3** was subjected to *in vitro* α-glucosidase enzyme inhibition assay, The results are presented in Table-4.

Compound **3** showed a potent α-glucosidase inhibition activity with IC_{50} values 305 ± 3.8 μM, and was found to be several fold more active than the standard drug, acarbose (IC_{50} = 840 ± 1.73 μM).

Apparently one of the enantiomers of the (±) mixture was responsible of activity in various biological bioassays.

3.4. Optimized molecular geometry

The structure of the studied molecule has been optimized using the B3LYP/6–311G(d,p) method. The optimized molecular geometry is shown in Fig. 4. The studied compound possesses C_1 point group. Selected optimized geometric parameters (bond lengths and bond angles) compared with the X-ray results are given in Table 2. The optimized geometric parameters showed a good agreement with the structural parameters obtained from the crystallographic information file (CIF). The calculated C–C–C bond angle values of the phenyl rings are in the range of 117.9–122.7° (exp. 117.6–123.0°) [44]. The calculations predicted the O1···H44, O2···H47 and O3···H19 intramolecular distances are 2.262 Å (exp. 2.358 Å), 2.260 Å (exp. 2.367 Å) and 2.316 Å (exp. 2.355 Å), respectively. These results indicate the presence of some intramolecular O … H interactions between the O-atoms of the pyrimidinetrione moiety and the H-atoms of the neighboring C–H bonds. Moreover, the studied compound has three six member rings, two are benzene and the third is the pyrimidinetrione. The calculated C–C–C–C dihedral angles of the two benzene rings are almost 0° indicating, commonly, the perfectly planar structure of these rings. In contrast, pyrimidinetrione ring is not planar where the N7, N8, C10, C11 and C12 atoms are almost lie in the same plane. The C13 lies above this plane where the C11–N7–C12–C13, and C11–N8–C10–C13 dihedral angles are in the range 10.4–11.1°.

3.5. Natural atomic charge

Distribution of positive and negative charges has vital role in the application of quantum chemical calculations to molecular system because of atomic charges affect dipole moment, molecular polarizability, electronic structure, acidity–basicity behavior and more lot of properties of molecular system. These electronic properties have strong relations to the biological activity of compound. The calculated natural charges (NAC) at the different atomic sites are given in Table 5. The carbonyl O–atoms are the most electronegative atomic sites in the molecule. The calculated natural charge densities at these atoms are in the range −0.5870 to −0.6093. The two oxygen atoms (O5 and O6) of the nitro group are less electronegative than the carbonyl oxygen. Also, the two N-atoms of the

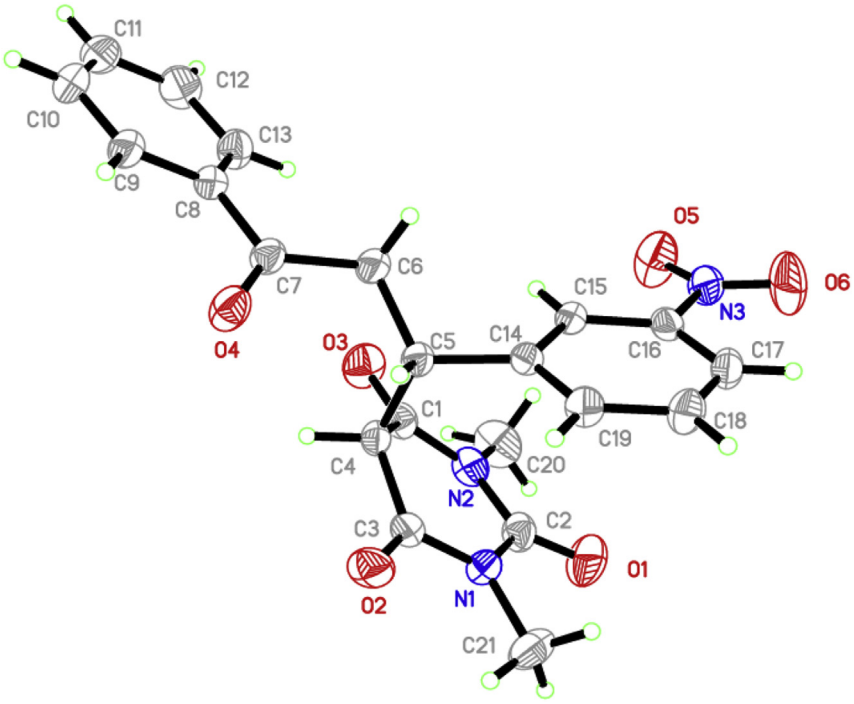

Fig. 2. ORTEP diagram of the compound **3**. Displacement ellipsoids are plotted at the 50% probability level.

pyrimidinetrione ring are electronrgative. In contrast, the N-atom of the nitro group has positive natural charge (0.5164). All the H–atoms are electropositive where the most electropositive H–site is H4a (0.2974). This H-atom affected strongly by the high electron withdrawing character of the two C═O groups surrounding it. The rest of H-atoms have natural atomic charge values in the range of 0.2000−0.2551. In contrast, the C-atoms have negative natural charges except C1, C2 and C3 which are bonded to O3, O1 and O2 atoms respectively. These carbonyl carbons have the highest positive NAC values.

3.6. Molecular electrostatic potential

Electrostatic potential map (MEP) is a very useful three dimensional diagrams used to visualize the charge distributions and charge related properties of molecules. The MEP picture is typically visualized through it values on the molecular electron density. It is a very useful property for analyzing and predicting

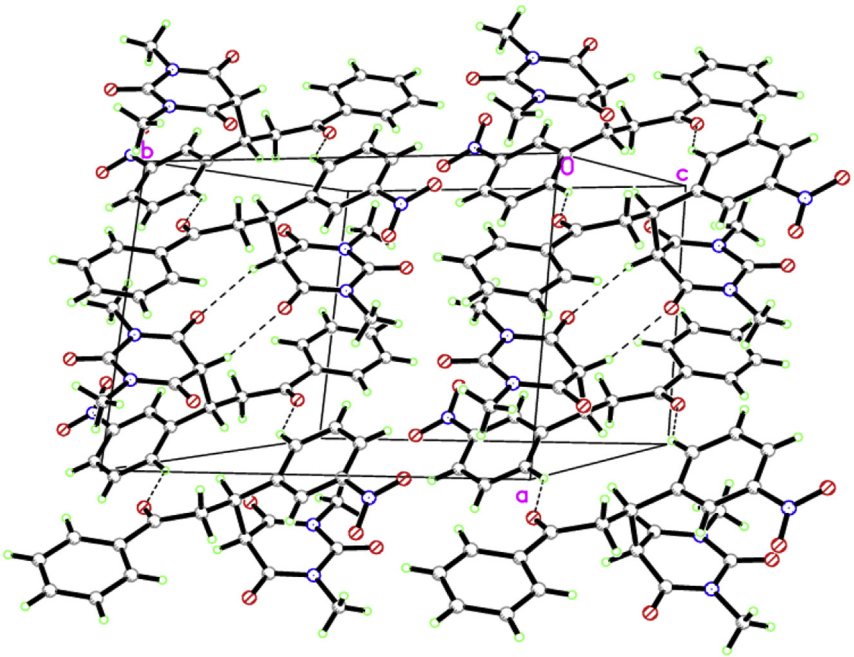

Fig. 3. Crystal packing showing intermolecular C–H…O hydrogen bonds as dashed lines.

Table 2
Comparison between the calculated and experimental geometric parameters.

Parameter	X-ray	DFT	Parameter	X-ray	DFT
O1–C2	1.208 (2)	1.210	N1–C3	1.379 (2)	1.391
O2–C3	1.210 (2)	1.212	N1–C21	1.464 (3)	1.472
O3–C1	1.214 (2)	1.215	N2–C1	1.369 (2)	1.387
O4–C7	1.211 (2)	1.220	N2–C2	1.396 (3)	1.402
O5–N3	1.216 (3)	1.223	N2–C20	1.465 (3)	1.473
O6–N3	1.213 (2)	1.224	N3–C16	1.468 (2)	1.482
N1–C2	1.385 (2)	1.398			
C2–N1–C3	123.89 (15)	125.17	N2–C1–C4	116.90 (16)	116.89
C2–N1–C21	117.74 (16)	115.75	O1–C2–N1	121.45 (19)	120.83
C3–N1–C21	118.32 (16)	119.00	O1–C2–N2	121.11 (19)	122.00
C1–N2–C2	124.15 (16)	125.03	N1–C2–N2	117.41 (16)	117.15
C1–N2–C20	117.90 (17)	117.14	O2–C3–N1	121.32 (16)	121.44
C2–N2–C20	117.84 (17)	117.75	O2–C3–C4	121.92 (16)	122.00
O5–N3–O6	122.44 (19)	124.72	N1–C3–C4	116.56 (15)	116.45
O5–N3–C16	119.21 (16)	117.75	O4–C7–C6	120.56 (16)	121.19
O6–N3–C16	118.35 (19)	117.53	O4–C7–C8	120.29 (15)	120.33
O3–C1–N2	121.33 (18)	121.44	N3–C16–C15	118.05 (16)	118.63
O3–C1–C4	121.67 (17)	122.00	N3–C16–C17	118.96 (15)	118.70

All e.s.d.'s (except the e.s.d. in the dihedral angle between two l.s. planes) are estimated using the full covariance matrix. The cell e.s.d.'s are taken into account individually in the estimation of e.s.d.'s in distances, angles and torsion angles; correlations between e.s.d.'s in cell parameters are only used when they are defined by crystal symmetry. An approximate (isotropic) treatment of cell e.s.d.'s is used for estimating e.s.d.'s involving l.s. planes.

molecular reactive behavior. In this regards, MEP picture has been used to predict the reactive sites for electrophilic and nucleophilic attack, and in studies of biological recognition and hydrogen bonding interactions [45,46]. Moreover, the MEP picture usually generated by overlapping the VdW radii of all atoms in the molecule so it reflects the molecule boundaries and it allows us to visualize the size and shape of molecules. MEP has been applied successfully to the study of interactions that involve a certain optimum relative orientation of the reactants. In order to predict the reactive sites for electrophilic and nucleophilic attack, the molecular electrostatic potential has been plotted for the title compound and is shown in Fig. 5. This figure provides a visual representation of the chemically active sites and comparative reactivity of atoms. Potential increases in the order red < orange < yellow < green < blue. Regions of negative potential (red) are usually associated with the lone pair of electronegative atoms while the positive electrostatic potential (blue) corresponds to the electropositive sites. It can

Table 3
Hydrogen-bond geometry (Å, °).

D—H…A	D—H	H…A	D…A	D—H…A
C4–H4A…O3[a]	0.9800	2.4700	3.415(2)	163.00
C5–H5A…O2[b]	0.9800	2.5900	3.407(2)	141.00
C6–H6B…O3	0.9700	2.3600	3.047(3)	128.00
C9–H9A…O6[c]	0.9300	2.5900	3.492(3)	163.00
C19–H19A…O4[b]	0.9300	2.5100	3.267(2)	138.00
C21–H21B…O6[d]	0.9600	2.5800	3.325(3)	135.00

Symmetry codes.
[a] −x+1, −y−1, −z.
[b] −x, −y−1, −z.
[c] x, y−1, z.
[d] −x, −y, −z.

Table 4
Result of α-glucosidase enzyme inhibition assay on compound **3**.

Compound	α-glucosidase inhibition (IC_{50} ± SEM [μM])
3	305 ± 3.8
Std.	Acarbose 840 ± 1.73

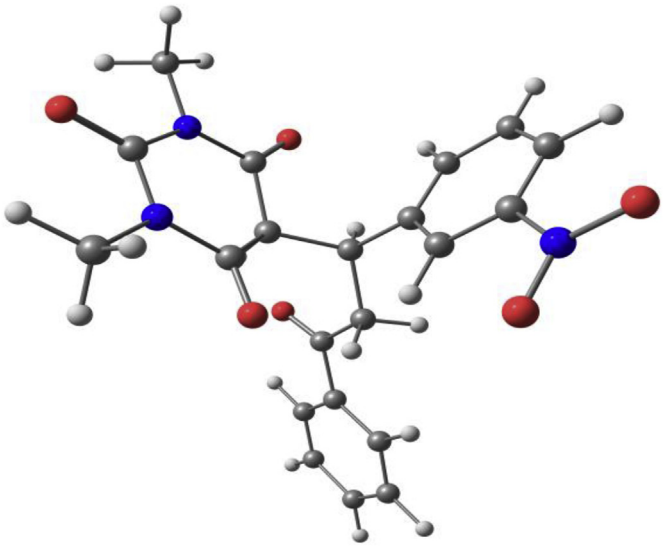

Fig. 4. The optimized molecular structure of the studied compound.

be seen from this figure that, negative regions (red) are mainly localized over the O-atoms. On other hand, the positive regions (blue) around the N-atom of the nitro group confirms the electron deficiency of this site. Moreover, the phenyl ring carrying the nitro group is less reactive toward the electrophilic attack compared to the other phenyl ring. The blue regions localized over the pyrimidinetrione ring indicate its high electron deficiency.

3.7. Nonlinear optical properties

Nonlinear optical materials were used as key materials for photonic communications which use light instead of electron for data transmission. With the development of laser technology, nonlinear optical materials have been extensively applied to industry, national defense, medicine and research [47,48]. Several organic materials were used for such applications. These organic compounds were characterized by their high polarizability (α_0) and low HOMO–LUMO gap (ΔE). The α_0 and ΔE values of the studied compound are calculated to be 261.73 $Bohr^3$ and 4.772 eV, respectively. The polarizability of the studied compound is 9 times higher than urea (28.00 $Bohr^3$). Also, the studied compound has lower energy gap (ΔE) compared to urea (7.66 eV). Based on these calculations, the studied molecule is considered as a better NLO material than this reference molecule used in literature [49].

3.8. Frontier molecular orbitals (FMOs)

The highest occupied molecular orbital (HOMO) and lowest unoccupied molecular orbital (LUMO) are called frontier molecular orbitals. The shapes of their electron densities and energies of have great interest for chemists and physicists. The shapes of these FMOs were used for predicting the most reactive position in π–electron systems and also explained several types of reactions in conjugated system [50]. Moreover, the energies of the lowest unoccupied molecular orbital (E_{LUMO}) and the highest occupied molecular orbital (E_{HOMO}) and their energy gap (ΔE) reflect the chemical reactivity of the molecule. A molecule having a small frontier orbital gap (ΔE) is more polarizable and is generally associated with a high chemical reactivity and low kinetic stability [51]. Recently the energy gap between HOMO and LUMO has been used to prove the bioactivity from intramolecular charge transfer (ICT) [52,53].

Table 5
The natural atomic charges calculated at the B3LYP/6-311G(d,p).

Atom	NAC	Atom	NAC
O1	−0.6025	C11	−0.1693
O2	−0.6006	H11A	0.2041
O3	−0.6093	C12	−0.1975
O4	−0.5870	H12A	0.2062
O5	−0.3834	C13	−0.1696
O6	−0.3852	H13A	0.2073
N1	−0.5011	C14	−0.0242
N2	−0.4981	C15	−0.2015
N3	0.5164	H15A	0.2551
C1	0.7273	C16	0.0682
C2	0.8498	C17	−0.1847
C3	0.7354	H17A	0.2371
C4	−0.3915	C18	−0.1857
H4A	0.2974	H18A	0.2108
C5	−0.2084	C19	−0.1635
H5A	0.2418	H19A	0.2234
C6	−0.4860	C20	−0.3548
H6A	0.2284	H20A	0.2072
H6B	0.2528	H20B	0.2238
C7	0.5997	H20C	0.2012
C8	−0.1499	C21	−0.3532
C9	−0.1470	H21A	0.2220
H9A	0.2234	H21B	0.2000
C10	−0.1972	H21C	0.2068
H10A	0.2056		

The E_{HOMO}, E_{LUMO} and ΔE values are calculated to be −7.316, −2.544 and 4.772, respectively. The HOMO and LUMO pictures are shown in Fig. 6. It is found that the HOMO level is mainly localized on the pyrimidinetrione moiety while the LUMO is located mainly on the benzoyl ring.

For understanding various aspects of pharmacological sciences including drug design and the possible biological characteristics of the drug molecules, several new chemical reactivity descriptors have been proposed. HOMO, which can be thought the outer orbital containing electrons, tends to give these electrons as an electron donor and hence the ionization potential is directly related to the energy of the HOMO. The ionization potential (I) is defined as the amount of energy required to remove an electron from the neutral molecule. Therefore, a high ionization potential indicates that the systems do not lose electrons with facility [54,55]. On the other hand, LUMO can accept electrons and the LUMO energy is directly related to electron affinity [56]. The electron affinity (A) is defined as the energy released when an electron is added to a neutral molecule. Using HOMO and LUMO orbital energies, the ionization energy and electron affinity can be expressed as: $I = -E_{HOMO}$ and $A = -E_{LUMO}$ [57]. Moreover, the hardness (η) is a measure of the resistance to charge transfer [58] while, the electronegativity is a measure of the tendency to attract electrons in a chemical bond, as is defined as the negative of the chemical potential in DFT [58]. The hardness (η) and chemical potential (μ) are given from the relations $\eta = (I-A)/2$ and $\mu = -(I + A)/2$, respectively [48]. The electrophilicity index (ω) measures the stabilization in energy when the system acquires an additional electronic charge from the environment. Parr et al. [59] proposed the global electrophilicity power as $\omega = \mu^2/2\eta$. Electrophilicity encompasses both the ability of an electrophile to acquire additional electronic charge and the resistance of the system to exchange electronic charge with the environment. It contains information about both electron transfer (chemical potential) and stability (hardness) and is a better descriptor of global chemical reactivity. For the title compound, the ionization potential I = 7.316, electron affinity A = 2.544, global hardness η = 2.386, chemical potential μ = −4.930, global electrophilicity ω = 5.093 eV. It is seen that the chemical potential of the title compound is negative and it means that the compound is stable. The hardness signifies the resistance towards the deformation of electron cloud of chemical systems under small perturbation encountered during chemical process. Soft systems are large and highly polarizable, while hard systems are relatively small and much less polarizable. The low value of chemical potential and high value of electrophilicity index for **3** favor its electrophilic behavior [60].

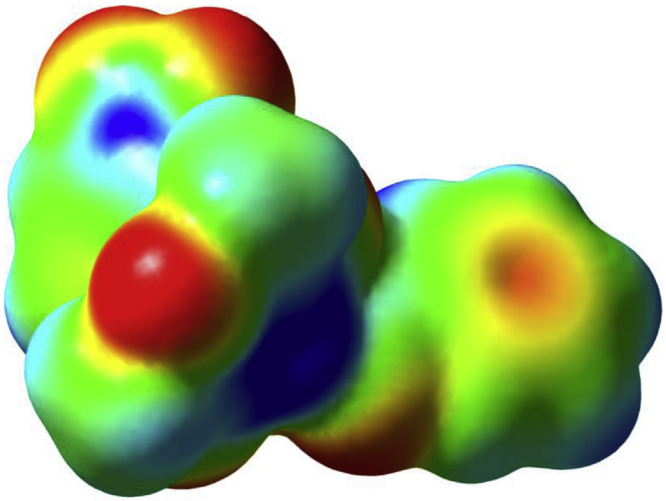

Fig. 5. Molecular Electrostatic potentials (MEP) mapped on the electron density surface calculated by the DFT/B3LYP method.

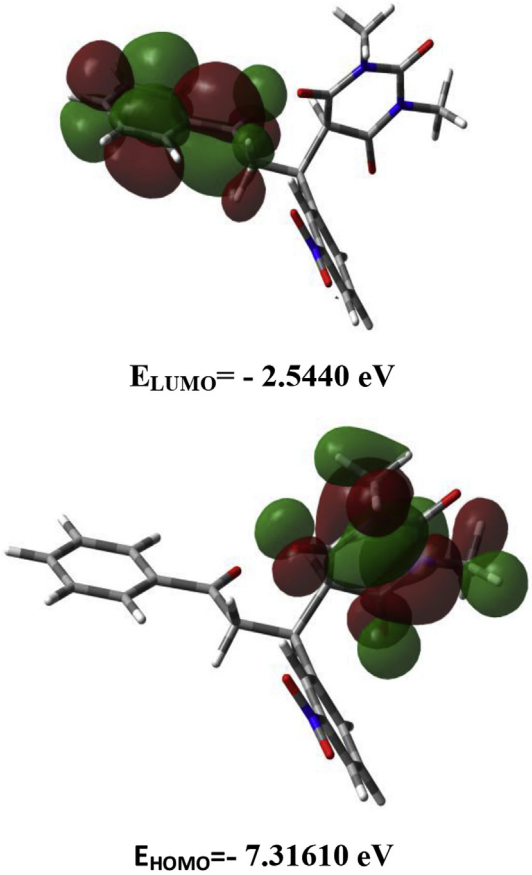

Fig. 6. The ground state isodensity surface plots for the frontier molecular orbitals.

3.9. Electronic spectra and TD-DFT calculations

The lowest energy electronic transition implies the electron transfer from the highest occupies molecular orbital (HOMO) to the lowest unoccupied molecular orbital (LUMO). The easiest way, but the less accurate, to calculate the energy of this transition is to calculate the energy gap between HOMO and LUMO levels. The HOMO–LUMO energy gap (ΔE) represents the lowest energy electronic transition. In the studied compound, the HOMO–LUMO energy gap is 4.772 eV. This electron transition belongs mainly to π–π* excitation which belongs to intramolecular charge transfer from the pyrimidine moiety to the benzoyl ring.

The accurate electronic transitions were calculated using the time–dependant density functional theory (TD–DFT). The spin allowed singlet–singlet electronic transitions calculated using the TD–DFT method were collected in Table S1 (Supplementary Information). The calculated electronic spectrum is shown in Fig. 7. On the basis of calculations, the studied compound showed intense electronic transition band at 243.9 nm (f = 0.2319) and a shoulder at 260.2 nm (f = 0.1483). These results showed good agreement with the observed electronic spectra in ethanol. The electronic transition band is due to H-4/H-2/H-1/H → L+2 electronic excitations while the shoulder is due to H-5 → L (76%) transition.

3.10. NMR spectra

The isotropic magnetic shielding (IMS) values calculated using the GIAO approach at the 6-311G(d,p) level are used to predict the ^{13}C and ^{1}H chemical shifts (δ_{calc}) for the studied compound and the results are correlated to the experimental NMR data (δ_{exp}) in $CDCl_3$ solvent. The experimental and theoretical values for ^{1}H and ^{13}C NMR chemical shifts of the studied compound are given in Table S2 (Supplementary Information). According to these results, the calculated chemical shifts are in compliance with the experimental findings. As shown in Fig. 8, good correlations between the experimental and the calculated chemical shifts for carbon ($R^2 = 0.928$) and proton ($R^2 = 0.998$) were obtained.

3.11. Natural bond orbital (NBO) analysis

The natural bond orbital (NBO) calculations were performed in order to understand various interactions between the filled NBOs of one bond and vacant orbitals of another one, which is a measure of the intramolecular delocalization of electrons. The stabilization

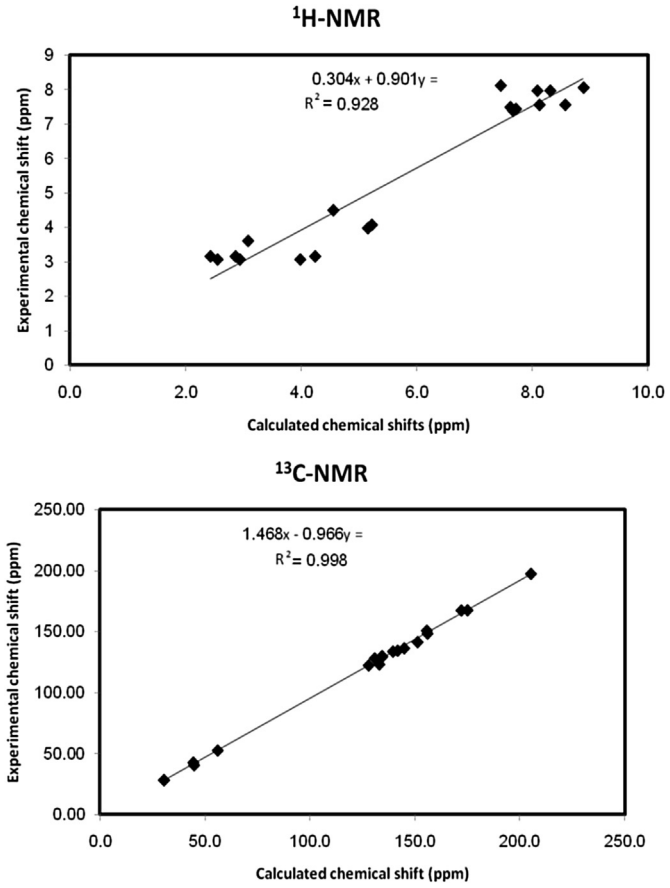

Fig. 8. The correlation graphs between calculated and experimental ^{1}H NMR and ^{13}C NMR chemical shifts of the studied compound **3**.

energies $E^{(2)}$ deduced from the NBO calculations for the most significant intramolecular charge transfer interactions are reported in Table 6. The larger the $E^{(2)}$ value, the more intensive is the interaction between electron donor and electron acceptor NBOs, i.e. the greater the extent of conjugation of the whole system [61]. The energy of these interactions can be estimated by the second–order perturbation theory [62]. The ICT interactions formed by the orbital overlap between π → π*, n → σ* and n → π* causing stabilization of the system upto 26.95, 25.98 and 165.36 kcal/mol respectively, which are due to BD(2)C16–C17 → BD*(2)O5–N3, LP(2)

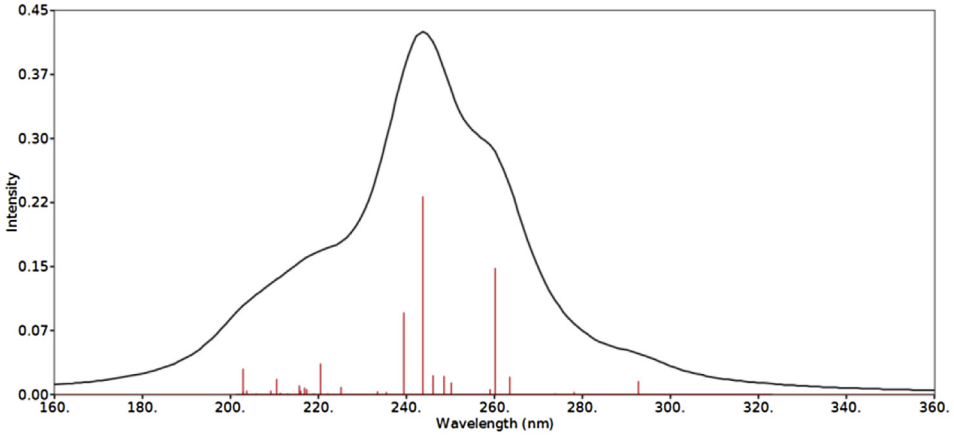

Fig. 7. The calculated electronic spectra of the studied compound **3** using TD-DFT method.

O3 → BD*(1)N2–C1 and LP(3)O6 → BD*(2)O5–N3 ICT interactions, respectively. These results indicate the presence of strong electron delocalization from LP(3)O6 to the neighboring O5–N3 bond. It is clear that, the ICT interaction energies due to the electron delocalization from the LP(2)O of the carbonyl groups to the BD*(1)C–H are very small indicating weak C–H … O intramolecular interactions.

3.12. Vibrational spectra

The vibrational frequencies of the titled compound were calculated by using the DFT B3LYP/6-311G(d,p) method. Vibrational mode assignments were made by visual inspection of the modes animated by using GaussView program [36]. Selected calculated vibrational frequencies are compared with the experimental vibrational frequencies (Table 7). The experimental and the predicted IR spectrum of the titled compound are given in Fig. 9. As can be seen from Table 6, there is good agreement between the experimental and calculated scaled IR vibrational frequencies [63].

3.12.1. Aromatic C–H vibrations

The hetero aromatic structure shows the presence of C–H stretching vibrations in the region 3100–3000 cm^{-1} [64]. In the present investigation, the IR bands identified for the C–H stretching vibrations at 3083 and 3066 cm^{-1} are calculated at 3124–3082 and 3077–3062 cm^{-1}, respectively. The bands corresponding to the in-plane and out-of-plane ring C–H bending vibrations are observed in the region 1400–1000 and 1000–600 cm^{-1} [65,66], respectively. In the present study, the DFT calculations predicted the in-plane bending modes at 1308–1251 cm^{-1} (exp. 1299 cm^{-1}) while the out of plane C–H bending modes are predicted at 975–745, 688 and 670 cm^{-1} (exp. 979–740, 688, 670 cm^{-1}).

Table 6
The second order perturbation energies $E^{(2)}$ (kcal/mol) of the most important charge transfer interactions (donor–acceptor) of the studied compound **3** using B3LYP method.

Donor NBO (i)	Acceptor NBO (j)	$E^{(2)}$kcal/mol
BD(1)C4–H4A	BD*(2)O2–C3	8.48
BD(1)C4–H4A	BD*(2)O3–C1	8.36
BD(2)C8–C13	BD*(2)O4–C7	19.33
BD(2)C8–C13	BD*(2)C9–C10	19.95
BD(2)C8–C13	BD*(2)C11–C12	18.58
BD(2)C9–C10	BD*(2)C8–C13	19.47
BD(2)C9–C10	BD*(2)C11–C12	21.88
BD(2)C11–C12	BD*(2)C8–C13	22.45
BD(2)C11–C12	BD*(2)C9–C10	17.87
BD(2)C14–C15	BD*(2)C16–C17	21.17
BD(2)C14–C15	BD*(2)C18–C19	21.13
BD(2)C16–C17	BD*(2)O5–N3	26.95
BD(2)C16–C17	BD*(2)C14–C15	21.16
BD(2)C16–C17	BD*(2)C18–C19	17.26
BD(2)C18–C19	BD*(2)C14–C15	19.28
BD(2)C18–C19	BD*(2)C16–C17	23.84
LP(2)O1	BD*(1)N1–C2	25.72
LP(2)O1	BD*(1)N2–C2	25.78
LP(2)O2	BD*(1)N1–C3	26.25
LP(2)O2	BD*(1)C3–C4	19.63
LP(2)O3	BD*(1)N2–C1	25.98
LP(2)O3	BD*(1)C1–C4	18.63
LP(2)O4	BD*(1)C6–C7	19.00
LP(2)O4	BD*(1)C7–C8	18.58
LP(2)O5	BD*(1)O6–N3	18.81
LP(2)O5	BD*(1)N3–C16	13.49
LP(2)O6	BD*(1)O5–N3	18.72
LP(2)O6	BD*(1)N3–C16	13.40
LP(3)O6	BD*(2)O5–N3	165.36
LP(1)N1	BD*(2)O1–C2	52.98
LP(1)N1	BD*(2)O2–C3	50.11
LP(1) N2	BD*(2)O1–C2	52.39
LP(1) N2	BD*(2)O3–C1	50.78
LP(2)O1	BD*(1)C20–H20B	0.58
LP(2)O2	BD*(1)C46–H47	0.60
LP(2)O3	BD*(1)C17–H19	0.69

Table 7
The calculated and experimental wavenumbers of the compound **3**.

Assignment	Calculated	Experimental
$\upsilon_{(CH,\ aromatic)}$	3124–3082, 3077–3062	3083, 3066
$\upsilon_{(CHasym,\ CH3)}$	3082–3081, 3031–2986	2979
$\upsilon_{(CHsym,\ CH3)}$	2966–2895	2954
$\upsilon_{(C{=}O)}$	1746–1675	1690
$\upsilon_{C{=}C}$	1608–1567	1591
$\upsilon_{(N{-}O,\ assym)}$	1550	1526
$\delta_{CHasymmethyl}$[a]	1473–1418	1449
$\delta_{(CH,\ sciss.)}$	1408	1379
$\delta_{CHsymmethyl}$[a]	1402, 1356, 1351	
$\delta_{(CH,\ wag.)}$	1354	
$\upsilon_{(N{-}O,\ sym)}$	1334	1347
$\delta_{CH\ aromatic\ in\ plane}$	1308–1251	1299
$\delta_{(CH,\ twist.)}$	1263, 1206	1210
$\upsilon_{(C{-}N)}$	1236	1271
Ring breathing	985, 984	998
$\delta_{CH\ aromatic\ out\text{-}of\text{-}plane}$	975–745, 688, 670	979–740, 688, 670
δ_{ONO}	860	885

υ: streching δ: bending.
[a] Mixed with other bending modes.

3.12.2. Aliphatic C–H vibrations

The C–H stretching vibrations of the methyl group occur at lower frequencies than those of the aromatic C–H ring vibrations [65]. The asymmetric stretch is usually at higher wavenumber than the symmetric one. The asymmetric C–H stretching modes of the methyl groups are calculated at 3082–3081 and 3031-2986 cm^{-1} (exp. 2979 cm^{-1}) while the C–H symmetric stretching vibrations are calculated at 2966–2895 cm^{-1} (exp. 2954 cm^{-1}). These results are in line with literature [65,67,68]. The asymmetric and symmetric bending vibrations of methyl groups usually appear in the region 1470–1440 cm^{-1} and 1390–1370 cm^{-1}, respectively [69,70]. These bending modes are predicted theoretically and observed experimentally in their characteristic regions mixed with other vibrations (Table 7). The calculations predicted the CH_2 scissoring, wagging and twisting vibrations at 1408 cm^{-1} (1379 cm^{-1}), 1354 cm^{-1} and 1263, 1206 cm^{-1} (1210 cm^{-1}) respectively.

3.12.3. C=O, C=C and C–N vibrations

The aromatic ring C=C stretching vibrations occur in the region of 1600–1500 cm^{-1} [65]. These stretching vibrations are observed at 1608–1567 cm^{-1} (exp. 1591 cm^{-1}). We noted, the aromatic ring breathing modes calculated at 985 and 984 cm^{-1} (exp. 998 cm^{-1}). The studied compound has four carbonyl vibrations predicted in the range 1746–1675 cm^{-1} (exp. 1690 cm^{-1}). Moreover the C–N stretching vibration band predicted theoretically and observed experimentally at 1236 $cm^{-1}$and 1271 cm^{-1} respectively [71].

3.12.4. N–O vibrations

The N–O symmetric and asymmetric stretching vibrations of the aromatic nitro compounds showed strong bands in the regions of 1530–1510 and 1360–1335 cm^{-1} [65]. The FTIR spectrum of the studied molecule showed these two strong bands at 1526 (calc. 1550) and 1347 (calc. 1334) cm^{-1} for the asymmetric and symmetric stretching vibrations of the N–O bonds respectively. The N–O bending vibration is detected at 885 cm^{-1} which is calculated using the DFT method at 860 cm^{-1}.

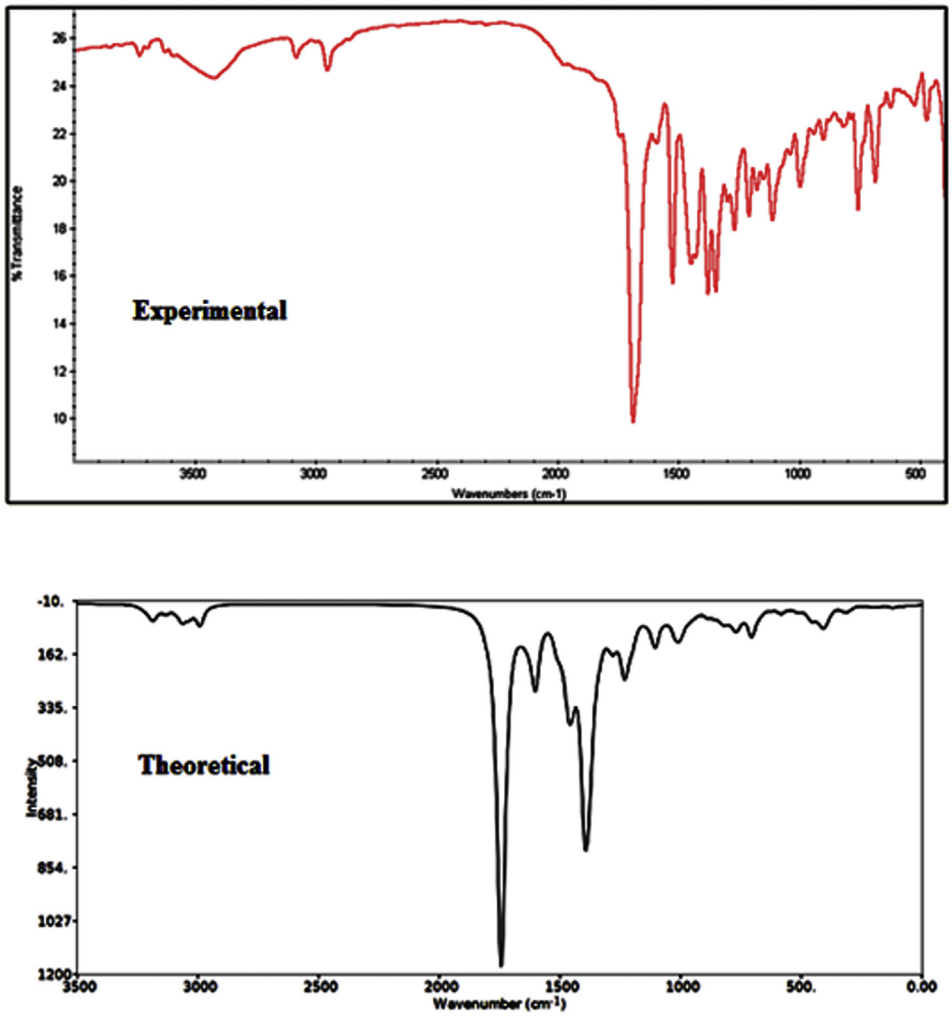

Fig. 9. The experimental (lower) and calculated (upper) infrared vibrational spectra of the studied compound.

3.13. Thermogravimetric analysis (TGA)

The TGA of the studied compound is performed over the temperature range 25–800 °C under a flowing nitrogenatmosphere and the result is shown in Fig. 10. The TGA data showed that the studied compound is thermally stable up to 181 °C then undergo sublimation without thermal decomposition in fast step leaving almost 0% residue.

3.14. Molecular docking study of compound **3**

Exploration of the molecular interaction of compound **3** with α-glucosidase enzyme was performed through molecular docking studies using MOE. Fig. 11 illustrated the predicted binding mode of compound **3** in the active site of α-glucosidase. From the docking study it was observed that compound **3** make four interaction (Three hydrogen side chain donor and one arene-cation interactions) with the active site residue (Acidic **Asp349**, Basic **Arg212** and **Arg439**) of α-glucosidase enzyme (Fig. 11), which may explain the fact that compound **3** possessed certain level of the inhibition. Asp349 and Arg212 were found in making H-bond (side chain donor) with the oxygen of 1,3-dimethylpyrimidine-2,4,6(1*H*,3*H*,5*H*)-trione moiety of the compound **3** and Arg439 was involved in making 2 interaction, one H-bond (with carbonyl oxygen) and another arene-cation (with phenyl ring) interaction with the active site of the enzyme.

4. Conclusion

In conclusion, we have synthesized a novel Michael adduct *via* Michael addition reaction using diethylamine as a base at room temperature. The TGA analysis showed high thermal stability of studied compound upto 181 °C. The molecular structure of compound **3** was optimized using the DFT/B3LYP method and 6-311G(d,p) basis set. The calculated bond distances and bond angles showed a good agreement with our reported X-ray crystal structure. The molecular electrostatic potential picture of the studied compound has been calculated using the same level of theory. The α_0 and HOMO-LUMO energy gap (ΔE) values indicated that the studied molecule is better NLO material than the urea. In accord with the experimental data, the TD–DFT calculated electronic showed intense electronic transition band at 243.9 nm (f = 0.2319) and a shoulder at 260.2 nm (f = 0.1483). The GIAO ^{1}H and ^{13}C NMR chemical shift values as well IR vibrational spectra correlated well with the experimental data. The correlation coefficients (R^2) for carbon and proton are 0.9957 and 0.9860, respectively. The Lewis structure NBOs as well as the different ICT interactions in the studied molecule have been predicted using the NBO calculations. Compound **3** was also evaluated for its biological activities in various *in vitro* biological assays. The potent α-glucosidase

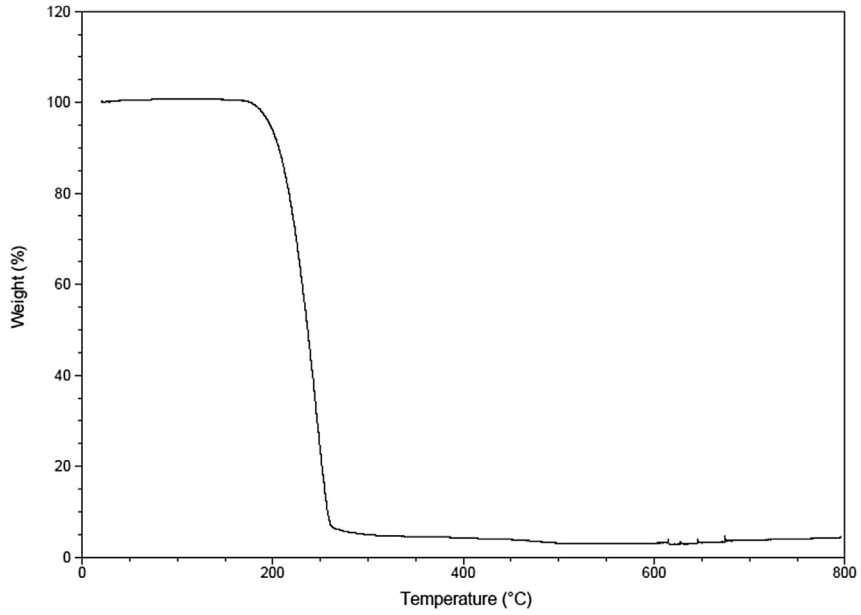

Fig. 10. The TGA curve of the studied compound **3**.

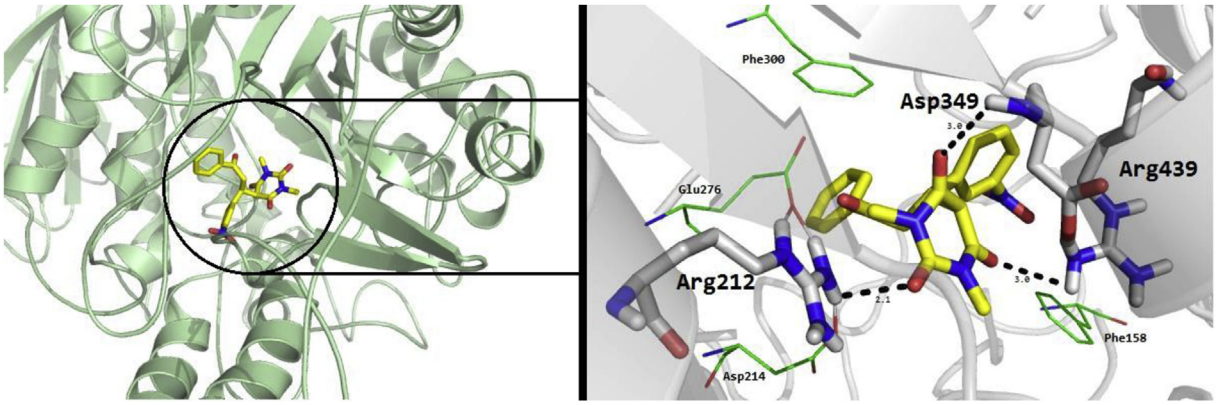

Fig. 11. Binding modes of compound **3** in the active site of a-glucosidase. Carbon atoms of the protein and the ligand are indicated in gray and yellow, respectively. Each dotted line indicates a hydrogen bond. (For interpretation of the references to color in this figure legend, the reader is referred to the web version of this article.)

inhibitory activity of compounds **3** indicated its potential as a treatment of possible leads for the treatment of hyperglycemia associated health disorders. Further studies towards the asymmetric synthesis of this compound are in process.

Acknowledgments

The authors would like to extend their sincere appreciation to the Deanship of Scientific Research at king Saud University for its funding this Research group NO (RG -257-1435-1436).

Appendix A. Supplementary data

Supplementary data related to this article can be found at http://dx.doi.org/10.1016/j.molstruc.2015.06.037.

References

[1] S. Sabatini, F. Gosetto, S. Serritella, G. Manfroni, O. Tabarrini, N. Iraci, J.P. Brincat, E. Carosati, M. Villarini, G.W. Kaatz, V. Cecchetti, J. Med. Chem. 55 (2012) 3568–3572.
[2] P. Min-Kyu, R. Yun-Hee, L. Hyo-Jung, L. Eun-Ok, K. Kwan-Hyun, P. Min-Jong, J. Byung-Hun, S. Bum-Sang, J. Chang-Hyun, C. Seung-Hoon, A. Kyoo-Seok, K. Sung-Hoon, Phytother. Res. 22 (2008) 58–64.
[3] N.R. Penthala, T.R. Yerramreddy, N.R. Madadi, P.A. Crooks, Bioorg. Med.Chem. Lett. 20 (2010) 4468–4471.
[4] L.S. Goodman, A. Gilman, in: The Pharmacological Basis of Therapeutics, McGraw-Hill, New Delhi, 1991, pp. 358–360.
[5] M.A.A. Radwan, E.A. Ragab, N.M. Sabry, S.M. El-Shenawy, Bioorg. Med. Chem. 15 (2007) 3832–3841.
[6] N.R. Madadi, N.R. Penthala, L.K. Brents, B.M. Ford, P.L. Prather, P.A. Crooks, Bioorg. Med. Chem. Lett. 23 (2013) 2019–2021.
[7] E. Maquoi, N.E. Sounni, L. Devy, F. Olivier, F. Frankenne, H.W. Krell, F. Grams, J.M. Foidart, A. Noël, Clin. Cancer Res. 10 (2004) 4038–4047.
[8] E. Milanesi, P. Costantini, A. Gambalunga, R. Colonna, V. Petronilli, A. Cabrelle, G. Semenzato, A.M. Cesura, E. Pinard, P. Bernardi, J. Biol. Chem. 281 (2006) 10066–10072.
[9] J.J.-W. Duan, Z.H. Lu, Z.R. Wasserman, R.Q. Liu, M.B. Covington, C.P. Decicco, Bioorg. Med. Chem. Lett. 15 (2005) 2970–2973.
[10] T.J. Hong, H. Park, Y.J. Kim, J.H. Jeong, J.S. Hahn, Bioorg. Med. Chem. Lett. 19 (2009) 4839–4853.
[11] G.E. Coggins, L. Maddukuri, N.R. Penthala, J.R. Hartman, S. Eddy, A. Ketkar, P.A. Crooks, R.L. Eoff, Chem. Biol. 8 (2013) 1722–1729.
[12] A. Barakat, A.M. Al-Majid, H.J. Al-Najjar, Y.N. Mabkhot, S. Javaid, S. Yousuf, M.I. Choudhary, Eur.J. Med. Chem. 84 (2014) 146–154.
[13] P.A. Evans, A. Grisin, M.J. Lawler, J. Am. Chem. Soc. 134 (2012) 2856–2859.
[14] J.-H. Xie, L.-C. Guo, X.-H. Yang, L.-X. Wang, Q.-L. Zhou, Org. Lett. 14 (2012) 4758–4761.

[15] C.F. Nisinga, S. Brase, Chem. Soc. Rev. 41 (2012) 988–999.
[16] A.G. Csaky, G.D.L. Herrana, M.C. Murcia, Chem. Soc. Rev. 39 (2010) 4080–4102.
[17] N.K. Rana, R. Unhale, V.K. Singh, Tetrahedron Lett. 53 (2012) 2121–2124.
[18] W. Yang, D.-M. Du, Org. Biomol. Chem. 10 (2012) 6876–6884.
[19] S.-J. Lee, S.-H. Youn, C.-W. Cho, Org. Biomol. Chem. 9 (2011) 7734–7741.
[20] D.L. Priebbenow, S.G. Stewart, F.M. Pfeffer, Org. Biomol. Chem. 9 (2011) 1508–1515.
[21] D. Enders, A. Saint-Dizier, M.-I. Lannou, A. Lenzen, Eur. J. Org. Chem. (2006) 29–49.
[22] S. Wen, P. Li, H. Wu, F. Yu, X. Liang, J. Ye, Chem. Commun. 46 (2010) 4806–4808.
[23] A. Barakat, A.M. Al-Majid, H.J. Al-Najjar, Y.N. Mabkhot, H.A. Ghabbour, H.-K. Fun, RSC Adv. 4 (2014) 4909–4916.
[24] A.M. Al-Majid, A. Barakat, H.J. Al-Najjar, Y.N. Mabkhot, H.A. Ghabbour, H.-K. Fun, Int. J. Mol. Sci. 14 (2013) 23762–23773.
[25] A. Barakat, A.M.A. Al Majid, M.S. Islam, Z.A. Al-Othman, Tetrahedron 69 (2013) 5185–5192.
[26] M.S. Islam, A.M. Al-Majid, Z.A. Al-Othman, A. Barakat, Tetrahedron Asymmetry 25 (2014) 245–251.
[27] A. Barakat, A.M. Al-Majid, H.J. Al-Najjar, M.I. Choudhary, S.S. Yousuf, Z. Kristallogr. –NCS 229 (2014) 269–270.
[28] A. Barakat, A.M. Al-Majid, Y.N. Mabkhot, H.A. Ghabbour, H.-K. Fun, Z. Kristallogr. –NCS 229 (2014) 235–236.
[30] A. Barakat, H.J. Al-Najjar, A.M. Al-Majid, S.M. Soliman, Y.N. Mabkhot, M. Rafi Shaik, H.A. Ghabbour, H.-K. Fun, Spectrochim. Acta 147 (2015) 107–115.
[31] A. Barakat, H.J. Al-Najjar, A.M. Al-Majid, S.M. Soliman, Y.N. Mabkhot, H.A. Ghabbour, H.-K. Fun, J. Mol. Struct. 1084 (2015) 207–215.
[32] A. Barakat, A.M. Al-Majid, H.J. Al-Najjar, S.M. Soliman, M.H.M. Al-Agamy, H.A. Ghabbour, H.-K. Fun, J. Mol. Struct. 1081 (2015) 519–529.
[33] G.M. Sheldrick, Acta Crystallogr. A 64 (2008) 112–122.
[34] G.M. Sheldrick, Shelxtl-pc (Version 5.1), Siemens Analytical Instruments, Inc., Madison, WI, 1997.
[35] M.J. Frisch, G.W. Trucks, H.B. Schlegel, G.E. Scuseria, M.A. Robb, J.R. Cheeseman, et al., Gaussian–03, Revision C.01, Gaussian, Inc., Wallingford, CT, 2004.
[36] T. Keith, J. Millam, GaussView, Version 4.1, R. Dennington II, Semichem Inc., Shawnee Mission, KS, 2007.
[37] G.A. Zhurko, D.A. Zhurko, Chemcraft: Lite Version Build 08 (Freeware), 2005.
[38] E.D. Glendening, A.E. Reed, J.E. Carpenter, F. Weinhold, NBO Version 3.1, CI,University of Wisconsin, Madison, 1998.
[39] S.B. Ferreira, A.C.R. Sodero, M.F.C. Cardoso, E.S. Lima, C.R. Kaiser, F.P. Silva, V.F. Ferreira, J. Med. Chem. 53 (2010) 2364–2375.
[40] J.-H. Park, S. Ko, H. Park, Bull. Korean Chem. Soc. 29 (2008) 921–927.
[41] A. Roujeinikova, C. Raasch, S. Sedelnikova, W. Liebl, W. Rice, J. Mol. Biol. 321 (1) (2002) 149–162.
[42] L.R. Guerreiro, E.P. Carriero, L. Fernandes, T.A. Cardote, R. Moreira, A.T. Caldeira, R.C. Guedes, A.J. Burke, Bioorg. Med. Chem. 21 (2013) 1911–1917.
[43] K. Yamamoto, H. Miyake, M. Kusunoki, S. Osaki, FEBS J. 277 (2010) 4205–4214.
[44] M. Kurt, S. Yurdakul, J. Mol. Struc. (Theochem) 730 (2005) 59–67.
[45] J.S. Murray, K. Sen, Molecular Electrostatic Potentials, Concepts and Applications, Elsevier, Amsterdam, 1996.
[46] E. Scrocco, J. Tomasi, Adv. Quantum Chem. 11 (1978) 115.
[47] P. Gnanasekaran, J. Madhavan, Asian J. Chem. 22 (2010) 109–114.
[48] V.M. Geskin, C. Lambert, J.L. Bredas, J. Am. Chem. Soc. 125 (2003) 15651–15658.
[49] L.S. Pu, Acs Symp. Ser. 455 (1991) 331–342.
[50] K. Fukui, T. Yonezawa, H.J. Shingu, A molecular–orbital theory of reactivity in aromatic hydrocarbons, J. Chem. Phys. 20 (1952) 722–725.
[51] N. Sinha, O. Prasad, V. Narayan, S.R. Shukla, J. Mol. Simul. 37 (2011) 153–163.
[52] L. Padmaja, C. Ravikumar, D. Sajan, I.H. Joe, V.S. Jayakumar, G.R. Pettit, F.O. Neilsen, J. Raman Spectrosc. 40 (2009) 419–428.
[53] C. Ravikumar, I.H. Joe, V.S. Jayakumar, Chem. Phys. Lett. 460 (2008) 552–558.
[54] J.B. Foresman, Æ. Frisch, Exploring Chemistry with Electronic Structure Methods, second ed., Gaussian, Pittsburgh, PA, 1996.
[55] R. Chang, Chemistry, seventh ed., McGraw-Hill, New York, 2001.
[56] B. Kosar, C. Albayrak, Spectrochim. Acta 78 (2011) 160–167.
[57] T.A. Koopmans, Physica 1 (1993) 104–113.
[58] R.G. Parr, W. Yang, Density-functional Theory of Atoms and Molecules, Oxford University Press, New York, 1989.
[59] R.G. Parr, L. Von Szentpály, S.B. Liu, J. Am. Chem. Soc. 121 (1999) 1922–1924.
[60] R.N. Singh, A. Kumar, R.K. Tiwari, P. Rawat, V.P. Gupta, J. Mol. Struct. 1035 (2013) 427–440.
[61] S. Sebastian, N. Sundaraganesan, Spectrochim. Acta Part A 75 (2010) 941–952.
[62] I. Hubert Joe, I. Kostova, C. Ravikumar, M. Amalanathan, S.C. Pinzaru, J. Raman, Spectrosc 40 (2009) 1033–1038.
[63] S.P.V. Chamundeeswari, E.R.J.J. Samuel, N. Sundaraganesan, Eur. J. Chem. 2 (2) (2011) 136–145.
[64] G. Varsanyi, Vibrational Spectra of 700 Benzene Derivatives, vols. (I–II), Akademici Kiaclo, Budapest, 1974.
[65] G. Socrates, Infrared and Raman Characteristic Group Frequencies, Tables and Charts, third ed., Wiley, Chichester, 2001.
[66] G. Varsanyi, Vibrational Spectra of Benzene Derivatives, Academic Press, New York, 1969.
[67] J. Sponer, P. Hobza, Int. J. Quant. Chem. 57 (1996) 959–970.
[68] N.B. Colthup, L.H. Daly, S.E. Wiberley, Introduction to Infrared and Raman Spectroscopy, Academic Press, New York, 1964.
[69] B. Smith, Infrared Spectral Interpretation, a Systematic Approach, CRC Press, Washington, DC, 1999.
[70] F.R. Dollish, W.G. Fateley, F.F. Bentley, Characteristic Raman Frequencies of Organic Compounds, John Wiley & Sons, New York, 1997.
[71] J.B. Lambert, H.F. Shurvell, D.A. Lightner, R.G. Cooks, Organic Struc. Spect, Simon & Schuster/A Viacom Company, New Jersey, 1998.